Cell Reports, Volume *21*

Supplemental Information

Association with Aurora-A Controls N-MYC-Dependent Promoter Escape and Pause Release of RNA Polymerase II during the Cell Cycle

Gabriele Büchel, Anne Carstensen, Ka-Yan Mak, Isabelle Roeschert, Eoin Leen, Olga Sumara, Julia Hofstetter, Steffi Herold, Jacqueline Kalb, Apoorva Baluapuri, Evon Poon, Colin Kwok, Louis Chesler, Hans Michael Maric, David S. Rickman, Elmar Wolf, Richard Bayliss, Susanne Walz, and Martin Eilers

Supplemental Experimental Procedures

CONTACT FOR REAGENT AND RESOURCE SHARING

Further information and requests for resources and reagents should be directed to and will be fulfilled by the Lead Contact, Martin Eilers (martin.eilers@biozentrum.uni-wuerzburg.de).

EXPERIMENTAL MODEL AND SUBJECT DETAILS

Cell culture

Neuroblastoma cell lines (IMR-5, IMR-32, SH-EP) were verified by STR profiling and grown in RPMI-1640 (Sigma-Aldrich and Thermo Fisher Scientific); HEK293TN and PlatE cells were grown in DMEM (Sigma-Aldrich and Thermo Fisher Scientific). Media were supplemented with 10% fetal calf serum (Biochrom) and penicillin/streptomycin (Sigma-Aldrich). All cells were routinely tested for mycoplasma contamination. For starvation experiments, IMR-5 cells were cultivated in serum-free medium for 48 h and then re-stimulated by change to media containing 10% fetal calf serum.

METHOD DETAILS

Transfection and lentiviral infection

For lentivirus production, HEK293TN cells were transfected using PEI (Polyethyleneimine, Sigma-Aldrich). Transfections of siRNAs were performed using RNAiMAX reagent and OptiMEM (Life Technologies) according to manufacturer's protocol. siRNAs used are listed in reference table. Cells were harvested 48 h after transfection. For production of stable SH-EP cell lines, PlatE cells were transfected with amino-terminal HA-tagged N-MYC expression plasmids. Retroviral supernatants were used for infection of SH-EP cells stably expressing the murine ecotropic receptor in the presence of 4 μg ml^{-1} polybrene (Sigma-Aldrich) for 24 h. Infected cells were selected with 3 μg ml^{-1} blasticidin for 2 weeks, clones were picked and expanded. Lentiviruses expressing a shRNA targeting TFIIIC5 (targeting sequence: AAGCGCAGCACCTACAACTACA), TFIIIC2 (targeting sequence:

TCCGTAGAGATGTCATTACCTA) or N-MYC (targeting sequence: GAGGAGCATGTTTTGTATACAA) were produced by transfection of pINDUCER-11 plasmid together with the packaging plasmid psPAX.2, and the envelope plasmid pMD2.G into HEK293TN cells. Virus-containing supernatant was harvested 24 h and 48 h after transfection. IMR-5 cells were infected with lentiviral supernatants in the presence of 4 μg ml^{-1} polybrene (Sigma-Aldrich) for 24 h. shRNA expression was stimulated by addition of doxycycline (1 μg ml^{-1}) for 12 h and cells were FACS-sorted for RFP-positive cells. Cells were harvested 48 h after induction with doxycycline (1 μg ml^{-1}) or ethanol as control.

For CRISPR-constructs guide-RNA (gRNA) were designed based on target sequences against TFIIIC5 reported in Hart et al. (Hart et al., 2015). Oligonucleotides were annealed and cloned into the BsmBI-BsmBI sites downstream from the human U6 promoter in the lentiCRISPR v2 plasmid. Lentivirus production and infection was done as described above. Cells were treated with 0.05 μg ml^{-1} of puromycin to select resistant cells.

Sequences of gRNA.

	Gene specific part TFIIIC5-exons
TFIIIC5-gRNA-1	CCCTGCCAGACGCACAGGGA
TFIIIC5-gRNA-2	GCTCATGCTCCGGCCCGAGA
TFIIIC5-gRNA-3	GAATCCATAGGCTGCGCCAG
TFIIIC5-gRNA-5	CATTTCGGGACCAGATGGGA
TFIIIC5-gRNA-6	GAGAACGAGGCGGCAGAAAG
TFIIIC5-gRNA-7	ATGGTGTGCGTGGAGTACCC
TFIIIC5-gRNA-8	ACCGACCAGAGACCCAGCAC

Clonogenic assay

IMR-5 and SH-EP cells expressing a doxycycline-inducible shRNA targeting shTFIIIC5 were seeded at low density and treated with doxycycline or ethanol as control until cells were confluent. Cells were fixed by adding 3.7% formaldehyde to the medium for 15 min. After removing the medium dishes were dried over night. 2 ml of 0.1% crystal violet staining solution was added and incubated for 2 h at room temperature. Dishes were washed in a stream of tap water. After washing dishes were inverted and dried over night.

Immunoblots and immunoprecipitations

Whole-cell extracts were prepared using NP-40 buffer (50 mM Tris (pH 8.0), 150 mM NaCl, 1% NP-40, and a cocktail of protease inhibitors) with three rounds of freeze/thaw cycles or RIPA buffer (50 mM HEPES, 140 mM NaCl, 1 mM EDTA; 1% Triton X-100, 0,1% Nadeoxycholate, 0,1% SDS) containing protease and phosphatase inhibitor cocktails (Sigma-Aldrich). Lysates were cleared by centrifugation, separated on SDS or Bis-Tris gels and transferred to a PVDF membrane (Millipore). Antibodies are listed in the resource table.

For immunoprecipitation, cells were re-suspended in lysis buffer containing 20 mM HEPES-KOH (pH 7.8), 140 mM KCl, 0.2 mM EDTA, 0.1% NP-40 supplemented with a cocktail of protease and phosphatase inhibitors. After brief sonication, samples were incubated on ice for 30 min and cleared by centrifugation. Co-immunoprecipitation was carried out in lysis buffer using 2 µg of antibodies and 1–2 mg lysate.

Flow cytometry analysis (FACS)

BrdU-PI-FACS was performed as described previously (Schulein-Volk et al., 2014). Subconfluent cells were labelled with 20 µM 5-Bromo-2'-deoxyuridine (BrdU, Sigma-Aldrich) for 1 h. Cells were harvested together with the supernatant, washed with ice-cold PBS and fixed in 80% ethanol overnight at -20 °C. Cells were washed with cold PBS and incubated in 2 M HCl/0.5% Triton X-100 for 30 minutes at room temperature. Cell pellets were neutralized by incubating with $Na_2B_4O_7$. The pellet was incubated with Anti-BrdU-FITC antibody diluted in 100 µl 1 % BSA, 0.5 % Tween-20 in PBS for 30 minutes at room temperature in the dark. After washing with PBS, the cells were re-suspended in PBS with RNAse A (24 µg ml^{-1}) and propidium iodide (PI, 54 µM) and incubated for 30 min at 37 °C.

For PI-FACS cells were harvested by trypsinization, washed with cold PBS and fixed in 80% ethanol overnight at −20 °C. After washing with PBS, the cells were re-suspended in PBS with RNAse A (24 µg ml^{-1}) and PI (54 µM) and incubated for 30 min at 37 °C. Subsequent analysis was performed on a BD FACSCanto II flow cytometer using BD FACSDIVA™ Software.

Mass spectrometric analysis

Proteins from immunoprecipitations were dissolved in NuPAGE LDS sample buffer (Life Technologies), reduced with 50 mM DTT at 70 °C for 10 min, alkylated with 120 mM iodoacetamide at room temperature for 20 min and separated on NuPAGE Novex 4-12% Bis-Tris gels (Life Technologies) with MOPS buffer according to manufacturer's instructions. Gels were stained for 45 min with Simply Blue™ Safe Stain (Life Technologies). Each gel lane was cut into 15 bands, gel bands were chopped and destained with 70% acetonitrile in 100 mM NH_4HCO_3 (pH 8), shrunk with 100% acetonitrile and dried in a vacuum concentrator (Concentrator 5301, Eppendorf). Dried gel pieces were suspended in 100 mM NH_4HCO_3 (pH 8) containing 0.1 µg trypsin (Trypsin Gold, Mass Spectrometry Grade, Promega) and proteins were digested overnight at 37 °C.

NanoLC-MS/MS analyses were performed on an LTQ-Orbitrap Velos Pro (Thermo Scientific) equipped with an EASY-Spray Ion Source and coupled to an EASY-nLC 1000 (Thermo Scientific). Peptides were loaded on a trapping column (2 cm x 75 µm ID. PepMap C18 3 µm particles, 100 Å pore size) and separated on an EASY-Spray column (25 cm x 75 µm ID, PepMap C18 2 µm particles, 100 Å pore size) with a 30-minute linear gradient from 3% to 30% acetonitrile and 0.1% formic acid. MS scans were acquired in the Orbitrap analyser with a resolution of 30,000 at m/z 400, MS/MS scans were acquired in the Orbitrap analyser with a resolution of 7,500 at m/z 400 using HCD fragmentation with 30% normalized collision energy. A TOP5 data-dependent MS/MS method was used. Lock mass option was applied for internal calibration in all runs using background ions from protonated decamethylcyclopentasiloxane (m/z 371.10124).

Mascot Distiller 2.4 (Matrix Science) was used for raw data processing and for generating peak lists with standard settings for the Orbitrap Velos. Mascot Server 2.4 was used for database searching with the following parameters: peptide mass tolerance: 8 ppm, MS/MS mass tolerance: 0.02 Da, enzyme: "trypsin" with three missed cleavage sites allowed for trypsin, fixed modification: carbamidomethyl (C), variable modifications: Gln->pyroGlu (N-term. Q) and oxidation (M). Database searching was performed against UniProt human

database. Spotfire was used to visualize data. Protein scores were calculated using MaxQuant (Cox and Mann, 2008).

In vitro binding assays

Constructs encoding FLAG-tagged fragments of the N-MYC transactivation domain were cloned into pETM6T1 and expressed as His-NusA fusions. These were purified on 5 ml chelating Sepharose columns (GE Healthcare) charged with nickel; the His-NusA tags were cleaved away using TEV NIa protease and removed by nickel affinity chromatography and the FLAG-N-MYC fragments were further purified by gel filtration using a Superdex 75 column (GE Healthcare) into N-MYC fragment buffer (20 mM HEPES pH 7.5, 100 mM NaCl). For *in vitro* pull-down assays from HeLa cell lysate, recombinant N-MYC fragments were immobilised on 30 µl Anti-FLAG M2 affinity gel (Sigma-Aldrich) and incubated with 1.2 mg of HeLa cell lysate in 150 mM sodium chloride, 50 mM Tris pH 8.0, 1.0% NP-40 and 1x Roche complete protease inhibitors. The final volume of the mix was made up to 495 µl with N-MYC fragment buffer. The concentration of FLAG-N-MYC fragments was determined by absorbance at 280 nm, however adjustments were made to account for differences observed in apparent concentration by immunoblots. The final protein concentrations were 9.3 µM for all fragments apart from N-MYC 1-137 (6.2 µM) and 46-89 (14.3 µM). The mixture was incubated by slow rotation at 4 °C for two hours prior to washing the gel three times with 500 µl N-MYC fragment buffer. FLAG-tagged fragments were eluted by addition of 85 µl of N-MYC fragment buffer with 0.25 mg ml^{-1} 3x FLAG-peptide (Sigma-Aldrich). This mix was allowed to rotate at 4 °C for 30 minutes prior to collection of eluates. Mixes and eluate fractions were subjected to SDS-PAGE and subsequently analyzed by immunoblotting. The competition assays were performed as described above with the exception that mixtures were spiked with either recombinant Aurora-A kinase or an equivalent amount of Aurora-kinase buffer. The recombinant Aurora-A protein used comprised residues 122-403 and C290A:C393A (Burgess and Bayliss, 2015). Expression and purification was performed as previously described (Bayliss et al., 2003). The protein was finally buffer exchanged by

repeated dilution and concentration into 150 mM NaCl, 20 mM HEPES pH 7.5, 5 mM $MgCl_2$, and 10% glycerol.

High-throughput sequencing

ChIP and ChIP-sequencing was performed as described previously (Walz et al., 2014). Cells were treated with 1% formaldehyde for 10 min at room temperature following 5 min of incubation with glycine. After cell lysis (5 mM PIPES pH 8.8, 5 mM KCl, 0.5% NP40), nuclei were re-suspended in RIPA buffer (50 mM HEPES pH 7.9, 140 mM NaCl, 1% Triton-X-100, 0.1% deoxycholic acid (DOC), 0.1% SDS, 1 mM EDTA containing protease inhibitor cocktail) and DNA was fragmented to a size <500 bp using a Branson sonifier. Antibodies were bound to Protein A/G-dynabeads (Invitrogen) and immunoprecipitated. Chromatin was eluted with 1% SDS and crosslinking was reverted overnight. Chloroform/phenol extraction was used for purification. ChIP-sequencing was performed as described before (Chen et al., 2008). Purified DNA was end-repaired, A-tailed, ligated to Illumina adaptors, size-selected (200 bp) and purified with Qiagen gel extraction kit. DNA fragments were amplified by 15-18 cycles of PCR and library size was tested with the Biorad Experion system. The amount of library DNA was quantified using a picogreen assay and subjected to Illumina GAIIx or Illumina NextSeq 500 sequencing according to the manufacturer's instructions. After base calling with the Genome Analyzer Data Collection Software, high quality PF-clusters (according to the CASAVA filter) were selected for further analyses. Antibodies are listed in the resource table. All ChIP-sequencing experiments were performed 1-3 times and results validated with independent ChIPs on individual genes.

Sequences of oligonucleotides for qPCR.

	forward	reverse
BIRC5 TSS	CTTTGAAAGCAGTCGAGGGG	TGTGCCGGGAGTTGTAGTC
BIRC5 TES	GGTCTGTGTTGAGAGGGTGA	GAAGTCAAGGCCCCAGTTTG
CDK14	CCCTCTCCTTCAATCCATCA	CGGAGCAGCAGAATCTGTAGT
CLINT1	GGCACTCTCAACGGTTTCTT	AAATTTATTGGGGAGGGGCG
EIF2B5	TTTTCGTTCCGCACCCTAAC	CTGAGAGCTGTTTCCACGTG
EIF3A	GAGAGGAGACGAAGGGGAAC	GCTCCTTCCTTTCCGTCTCT
EIF4H	CAGCTCTCCAGGTCACCTC	CTACGCGGCCCATTATGTG
ERCC	CCTCACTATCATCCATCCGCT	AGGTTTCCCAGGCCTACTC

GALNT14 (N-MYC binding)	AATGTGCTCGTCCTACCACA	AGTAGCCAGGCAAGTGAACC
GALNT14	CTAGACCCAGGATCCGGTTG	CAGGCTCGCTTCTCTTCGA
GLN3 TSS	GTGACGCTCGTCAGTGG	CATATTGGCTGTAGAAGGAAGC
GLN3 TES	GTTATGGTATGCATGAGCTGTG	CTACTTCCACTCACAATGAGATG
Intergenic region (chr3)	TATGTTGCTGTCCACCCCAT	TATCTGTGTAGGCCAGGCTG
Intergenic region (chr5)	GAGGCCAGTGGAAAGAGACA	TCTTTAACCCACTGCCACCT
Intergenic region (chr6)	GGGCTGGATATGCAGTGGTA	CCTCTTTCCTTGTATATGGCTCC
Intergenic region (chr14)	CCTTCTCCTCCTTCAGCTCC	CTCTCTGGCCTGTTTCCTCA
Intergenic region (chr16)	GGAAGACACCTGTTGCCAAG	TCACAGGCAGATGGTTAGGC
Intergenic region (chr21)	CTTTCCCAGGGCGCCATC	GGCATCCCCGAGTCAGAC
Intergenic region	CACACGAGGGTCCATAACGT	GTGGATTTCAGAGCCATCCG
LDHA TSS	GGAGGGCAGCACCTTACTTA	GTGGAACAGCTATGCTGACG
LDHA TES	TGTGGAATCTTTTGCTTTCCCT	TGTTGGCCATGCTAGTCTTG
LHFPL	GCCATGCCTCAGTATCTCCT	GAACTTCAGTATCGGCCACC
MEI4	GCCATGCCTCAGTATCTCCT	TAAGACCCAACCGCCAGTAG
METAP1	AGGGAGGGCAGATGTGAATC	TCTTCACTGACGAACACCCA
Negative region (chr1)	GCAGTTCAACCTACAAGCCAATAGAC	CACAAATTAGCGCATTGCCTGA
Negative region (chr11)	TTTTCTCACATTGCCCCTGT	TCAATGCTGTACCAGGCAAA
NCL TSS	CTACCACCCTCATCTGAATCC	TTGTCTCGCTGGGAAAGG
NCL TES	AGCCTTCATCCAGGTGAGAA	GGCCACACGGCATATAGACT
NME1 TSS	GGGGTGGAGAGAAGAAAGCA	TGGGAGTAGGCAGTCATTCT
NME1 TES	GATTGCTGAGGTGCTTGGAG	AGCAACTCAAGAGGCTGAGT
NPM1 TSS	TTCACCGGGAAGCATGG	CACGCGAGGTAAGTCTACG
NPM1 TES	TAGGGCGTGGGTCTTTTCTT	AACTTGGGACCTCTACTGCC
PLK1	GTTTGAATTCGGGGAGGAGC	CAGTCACTGCAGCACTCATG
PPRC1 (N-MYC binding	GAAGGCTGAGACCTCCATGT	GTTCTCCCGGGAAAATTGCT
PPRC1	GTGAGGATTAGCGCTTGGAG	TGCTGACGTTCCTTTCACC
RCC1 TSS (N-MYC binding	AGTGGTCGCTTCTTCTCCTT	GCATTAGACCCACAACTCCG
RCC1 TSS	GTAGCTGGGACTGGAGGTG	TTGAGGCCAGGAGTTCGAG
RCC1 TES	TGTGGTATGGGACTGTGCAA	ACTCCTGACCTCAAGCGATC
tRNA119Ala	ACTTGTGCCAGGGGATGTAG	AATCTACGTGATCGCCTTGG
tRNA7Leu	ATGTAGCATAAGCGCGTCAG	ACTGTCAGGAGTGGGATTCG

RNA-sequencing was performed as described previously (Jaenicke et al., 2016) using an Illumina NextSeq 500. RNA was extracted using RNeasy mini columns (Qiagen) including on-column DNase I digestion. mRNA was isolated using the NEBNext® Poly(A) mRNA Magnetic Isolation Module (NEB) library preparation was performed with the NEBNext®

Ultra™ RNA Library Prep Kit for Illumina following the instruction manual. Libraries were size-selected using Agencourt AMPure XP Beads (Beckman Coulter) followed by amplification with 12 PCR cycles. Library quantification and size determination was performed with the Experion Automated Electrophoresis System (Bio-Rad).

Peptide microarrays

For evaluation in microarray format Myc peptides were synthesized in parallel using a ResPep SL synthesis robot (Intavis AG) equipped with a Celluspot synthesis module and printed using a slide spotting robot (Intavis AG). Total synthesis time was 256 h. Coupling reagents were freshly prepared every 48 h. Synthesis was based on Standard Fluorenylmethoxycarbonyl (Fmoc) peptide synthesis using reagents from Sigma-Aldrich and Iris and performed on acid-soluble Fmoc-β-Alanine etherified cellulose disks (area 0.12 cm^2, loading 1.0 µmol cm^{-2}). N-terminal Fmoc protection was removed by adding 2 µl and 4 µl 20% Piperidine in N-Methyl Pyrrolidone (NMP) for 5 and 10 min. Four couplings (10, 20, 30 and 40 min) using Oxyma/N,N′-Diisopropylcarbodiimide/Amino Acid in the relation (1.1/1.5/1.0) in at least 5-fold excess followed by two washing steps (100 µl and 300 µl NMP) and 4 µl capping solution (5% Acetic Anhydride in NMP) achieved peptide elongation by one amino acid. The subsequent peptide work-up was performed manually on all peptides in parallel after transfer of the cellulose disks into 96 deep-well blocks. Peptide side-chain deprotection was achieved with 150 µl deprotection solution (trifluoroacetic acid/triisopropylsilane/water/DCM: 80%, 3%, 5%, 12%) for 2 h. Disks were then solubilized overnight in 250 µl of cellulose solvation solution (trifluoroacetic acid/trifluoromethansulfonic acid/triisopropylsilane/water: 88.5%, 4%, 2.5%, 5%) under strong agitation. 750 µl Diethylether (-20° C) was added to the dissolved cellulose−peptide conjugates. The mixture was briefly agitated and kept at -20 °C for 1 h. Precipitated conjugates were pelleted by centrifugation at 2,000 rcf for 30 min at 4 °C. After removal of the supernatant the pellet was additionally washed twice with 750 µl fresh Diethylether (-20° C). After the final washing step, residual ether was evaporated and 250 µl of dimethyl sulfoxide (DMSO) was added to re-

solvate the cellulose-peptide conjugates. The cellulose-peptide conjugate stock solutions were stored at -20 °C. Prior printing 80 µl of the stocks were transferred to a 384-well plate, and mixed with 20 µl SSC buffer (150 NaCl; 15 µM $Na_3C_6H_5O_7$; pH 7.0). 50 nl of each peptide was contact printed on coated glass slides with a slide spotting robot (Intavis AG).

After drying overnight, peptide microarrays were washed, equilibrated and blocked with 2 x 2 ml array buffer (0.01 M phosphate buffered saline (NaCl 138 mM; KCl 2.7 mM); pH 7.4, 0.05% bovine serum albumin). Arrays were incubated with 2 ml Aurora-A kinase at 4 °C for 1 h. After washing with 4 x 2 ml array buffer the arrays were incubated with 2 ml array buffer and horse radish peroxidase (HRP) coupled anti-His antibody (Thermo Fisher Scientific, MA1-21315-HRP, dilution 1:20,000). Aurora-A kinase binding was visualized after washing with 4 x 2 ml array buffer with 300 µl ECL Western Blotting Substrate (Thermo Fisher Scientific). Prepared microarrays were imaged using the GeneSys Pxi system (Syngene). The resulting images were analyzed using the Active Motif software. For all peptide array data sets >95% of the peptide SPOTs were within an <5% error margin when comparing intensities between peptide duplicates.

QUANTIFICATION AND STATISTICAL ANALYSIS

Bioinformatic analyses and statistics

Base calling was performed with Illumina's CASAVA software or FASTQ Generation software v1.0.0 and overall sequencing quality was tested using the FastQC script. For ChIP-sequencing, fastq files were mapped to the human genome (hg19) using Bowtie v1.1.1. (Langmead and Salzberg, 2012) with default parameters and normalized to the sample with the smallest number of mapped reads. Peaks were called using MACS v1.4.2 (Zhang et al., 2008) with a p-value cut-off of $1.0x10^{-6}$ (N-MYC, TFIIIC5), $1.0x10^{-11}$ (RAD21) or $1.0x10^{-12}$ (CTCF) and the input sample as control. Wiggle files were generated using MACS, bedGraph files were generated using the genomecov function from BEDTools and the Integrated Genome Browser (Nicol et al., 2009) was used to visualize density files. Heat maps illustrating DNA binding were calculated using DeepTools (Ramirez et al., 2016) with a resolution of 50 bp. Overlapping N-MYC/TFIIIC binding sites were determined using the intersectBed function from BEDTools (Quinlan, 2014) with a minimum overlap of 1 bp and corresponding p-values were calculated using a permutation test with $1.0x10^{6}$ iterations. Genes were assigned to be bound by N-MYC or TFIIIC, if a peak was called within a region of +/-1 kb around a transcriptional start site.

N-MYC binding sites were generated by intersecting N-MYC peaks in DMSO and CD532 using bedtools with a minimum overlap of 1 bp leading to 10,157 peaks. TFIIIC5 reads in +CD532 sample were counted in a region of +/-100 bp around the N-MYC peak summit and binding sites with less then 8 reads were defined as N-MYC-only sites. Only binding sites that were within +/-1 kb around a transcriptional start site of an RNAPII transcribed gene were considered. To determine the occupancy of N-MYC, TFIIIC5, CTCF and RAD21 the number of reads was counted in a region of +/-100 bp around the N-MYC peak summit.

Changes in N-MYC and TFIIIC occupancy upon CD532 treatment at N-MYC/TFIIIC peaks was calculated by counting tags in a region of 50 bp around the N-MYC peak, p-values were calculated using a two-tailed one-sample Wilcoxon signed-rank test. Occupancy at promoters of selected gene sets was measured by counting tags in a region of +/-0.5 kb

around the TSS and corresponding p-values were calculated by a two-tailed, paired Wilcoxon signed-rank test.

For *de novo* motif analyses of N-MYC and TFIIIC peaks the MEME and DREME algorithms implemented in the MEME Suite (Bailey et al., 2009) were used with an input region of +/- 50 bp around the peak summit. To compute occurrences of pre-defined motifs (E-box: CACGTG, CTCF: MA0139.1, AP2a: MA0003.2) the CENTRIMO tool was used: the frequency of a motif at a certain position was normalized to the number of input sequences and a rolling mean of 20 bp was applied for smoothing the curves.

RNAPII occupancy was calculated by counting reads in promoters (-30 bp to +300 bp relative to TSS), gene bodies (+300 bp to TES) and TES (TES to +1 kb), addition of one pseudocount/kb and normalization to region length. The traveling ratio is defined as occupancy in promoter divided by occupancy in gene body (Rahl et al., 2010). For the analyses only expressed/RNAPII-bound genes were used (2D Kernel density plots: >20 RNAPII counts/kb in promoters; bin plots: $\log_2$CPM >1.28). 2D Kernel density plots were generated with the smoothScatter function in R and default settings, bin plots were generated by calculating the mean of equal-sized bins. Metagene window plots were produced using ngs.plot (Shen et al., 2014) and all annotated genes from the UCSC RefSeq list.

For RNA-sequencing, reads were mapped to hg19 with TopHat2 (Kim et al., 2013) and Bowtie1 with default settings. Reads per gene were counted using the countOverlaps function from the R package *GenomicRanges*. Weakly expressed genes (mean count over all samples <1.5) were removed and differentially expressed genes were called using EdgeR. For Venn diagrams, genes were filtered based on $\log_2$FC threshold of |0.5| (siTFIIIC5 vs siCtr) or |1.0| (siRAD21 vs siCtr). Statistical significant overlap of regulated genes presented in Venn diagrams were calculated using a Monte-Carlo simulation with 100,000 iterations and 17,450 genes as population size. The p-values were calculated as (r+1)/(n+1) with r as the number of iterations producing a greater or equal overlap than the actual one and n as the total number of iterations (North et al., 2002). GSE analyses (Subramanian et

al., 2005) were performed with signal2noise metric, 1,000 permutations and the C2 gene set collection of MSigDB. To measure gene expression changes in N-MYC depleted neuroblastoma cells (GSE39218, samples with double infection) raw data were downloaded, RMA-normalized, probes to genes collapsed by mean and $\log_2$ fold changes were calculated. Association of gene expression of specific gene sets in human neuroblastoma was determined as described previously (von Eyss et al., 2015). Expression data at different stages were downloaded from GEO (GSE16476), RMA-normalized and the association score was calculated using a custom R script using the following formula: -log10 p-value x direction. Here, -1 means a negative and +1 a positive association. Box and whisker plots are characterized by a horizontal line reflecting the median, boxes spanning the first and third quartile and whiskers expanding to 1.5x interquartile range of the first and third quartile, respectively. Outliers are shown as individual dots, p-values comparing medians in box plots are calculated with one- or two-sample two-tailed Wilcoxon Signed-rank tests. For binned data the mean of each bin is plotted.

Statistical significance between experimental groups were determined by Student's t test or, when means of three or more groups were compared, by one-way ANOVA. Data analysis was performed with Prism5.0 Software (GraphPad). P values < 0.05 were considered statistically significant.

DATA AND SOFTWARE AVAILABILITY

ChIP- and RNA-sequencing datasets are available at the Gene Expression Omnibus under the accession number GEO: GSE78957. The authors do not declare a conflict of interest

Resource Table

REAGENT or RESOURCE	SOURCE	IDENTIFIER
Antibodies		
Actin beta (mouse)	Sigma-Aldrich	Clone: AC15 Cat# A5441
Aurora-A/AIK antibody (rabbit)	Cell Signaling	Cat# 3092
Aurora-A (rabbit)	Genetex	Clone: C3 Cat# GTX104620
Aurora-A (mouse)	Sigma-Aldrich	Clone: 35C1 Cat#A1231
Aurora-A (goat)	Santa Cruz	Clone: N-20 Cat# sc-14318
pT288 Aurora-A (rabbit)	Cell Signaling	Cat# 2914
ATM pS1981 (mouse)	Millipore	Clone: 10H11.E12 Cat# MAB3806
CDK2 (rabbit)	Santa Cruz	Clone: M-2 Cat# sc-163
CTCF (rabbit)	Abcam	Cat# ab70303
FLAG-tag (mouse)	Sigma-Aldrich	Clone: M2 Cat# F1804
HA-tag (rabbit)	Abcam	Cat# ab9110
N-MYC (mouse)	Santa-Cruz	Clone: B8.4.B Cat# sc-53993
N-MYC (mouse)	Calbiochem	Clone: NCM II 100 Cat# OP13
P400 (rabbit)	Abcam	Cat# ab5201
RAD21 (rabbit)	Bethyl	Cat# A300-080A
TFIIIC1 (mouse)	Santa Cruz	Clone: F-12 Cat# sc-398780
TFIIIC2 (mouse)	Abcam	Cat# ab89113
TFIIIC5 (rabbit)	Bethyl	Cat# A301-242A
TRRAP (rabbit)	Abcam	Cat# ab73546
TOP1 (rabbit)	Bethyl	Cat# A302-589A
TOP2A (rabbit)	Bethyl	Cat# A300-054A
TOP2B (rabbit)	Bethyl	Cat# A300-949A
Tubulin beta (mouse)	Millipore	Clone: TU-20 Cat# MAB1637
Vinculin (mouse)	Sigma-Aldrich	Clone: hVin-1 Cat# V9131
RPA32 (mouse)	Santa Cruz	Clone: MA34 Cat# sc-53496

RPA32 pS33 (rabbit)	Bethyl	Cat# A300-246A
RPA32 pS4/8 (rabbit)	Bethyl	Cat# A300-245A
CHK1 (rabbit)	Santa Cruz	Clone: FL-476 Cat# sc-7898
pS345 CHK1 (rabbit)	Cell Signaling	Clone: 133D3 Cat#2348
P53 (mouse)	Millipore	Clone: pAb1801 #Cat OP09
BRCA1 (rabbit)	Bethyl	Cat# A300-000A
RPA70 (mouse)	Millipore / Calbiochem	Clone: RPA34-20 Cat# NA19L
CDC73 (rabbit)	Bethyl	Cat# A300-170A
CTR9 (rabbit)	Bethyl	Cat# A301-395A
TRRAP (rabbit)	Bethyl	Cat# A310-373A
FITC anti-BrdU, Mouse IgG1, kappa	Biozol / BioLegend	Clone: 3D4 Cat# BLD-364104
RNA polymerase II (rabbit)	Santa Cruz	Clone: N-20 Cat# sc-899
RNA polymerase II CTD repeat YSPTSPS (phospho Ser2) (rabbit)	Abcam	Cat# ab5095
RNA polymerase II (hypo-phosphorylated) (mouse)	Santa Cruz	Clone: 8WG16 Cat# sc-56767
RNA polymerase II (phospho Ser5) (mouse)	BioLegend / previous Covance	Clone: CTD4H8 Cat# MMS-128P
Anti-rabbit HRP	Amersham	Cat# NA934
Anti-mouse HRP	Amersham	Cat# NA931
Rabbit TrueBlot	Rockland	Clone: eB182 Cat# 18-8816-33
Mouse TrueBlot	Rockland	Clone: eB182 Cat# 18-8816-33
IRDye® 800CW Donkey anti-Mouse IgG (H + L)	LI-COR Biosciences GmbH	Cat# 926-32212
IRDye® 800CW Donkey anti-Rabbit IgG (H + L)	LI-COR Biosciences GmbH	Cat# 926-32213
6x-His Tag Monoclonal Antibody (mouse)	Thermo Fisher Scientific	Clone: HIS.H8 Cat# MA1-21315

Chemicals, Peptides, and Recombinant Proteins		
MK-5108	Selleckchem	Cat# S2770
MLN8237	Selleckchem	Cat#S1133
CD532	R. Bayliss	N/A

CD532	Calbiochem / Merck	Cat# 532605
Thymidine	Sigma-Aldrich	Cat# T9250
3x FLAG-peptide	Sigma-Aldrich	Cat# F4799
Aurora-A protein	Burgess and Bayliss, 2015	N/A
Hoechst 33342	Sigma-Aldrich	Cat# B2261
4-Hydroxytamoxifen	Sigma-Aldrich	Cat# H7904-5MG
Puromycin	InvivoGen	Cat# ant-pr-1
MG-132	Calbiochem	Cat# 474790-20MG
Polybrene	Sigma-Aldrich	Cat# 107689-100G
Dynabeads® Protein A	Life Technologies GmbH	Cat# 10002D
Dynabeads® Protein G	Life Technologies GmbH	Cat# 10004D
Pierce® Anti-HA Agarose	Pierce	Cat# 26181
Pierce® HA Peptide	Pierce	Cat# 26184
Formaldehyde (37%)	Roth	Cat# 4979.1
Crystal Violet	Sigma-Aldrich	Cat# C0775-25G
Critical Commercial Assays		
Duolink® In Situ PLA® Probe Anti-Rabbit PLUS, Affinity purified Donkey anti-Rabbit IgG (H+L)	Sigma-Aldrich	DUO92002
Duolink® In Situ PLA® Probe Anti-Mouse MINUS, Affinity purified Donkey anti-Mouse IgG (H+L)	Sigma-Aldrich	DUO92004
Duolink® In Situ Detection Reagents Red	Sigma-Aldrich	DUO92008
Duolink® In Situ Wash Buffers, Fluorescence	Sigma-Aldrich	DUO82049
Rneasy Mini Kit	Qiagen	74106
Rnase-free Dnase kit	Qiagen	79254
MiniElute PCR Purification Kit	Qiagen	28006
QIAquick PCR Purification Kit	Qiagen	28106
QIAquick Gel Extraction Kit	Qiagen	28704
Experion RNA StdSense kit	Bio-Rad	700-7103
Experion DNA 1K Kit	Bio-Rad	700-7307
NEBNext® Ultra™ RNA Library Prep Kit for Illumina	NEB	E7530 L
NEBNext Poly(A) mRNA Magnetic Isolation Module	NEB	E7490 L
NEBNext® ChIP-Seq Library Prep Master Mix Set for Illumina®	NEB	E6240 L
NEBNext® Multiplex Oligos for Illumina® (Dual Index Primers Set 1)	NEB	E7600 S
NextSeq® 500/550 High Output Kit v2 (75 cycles)	Illumina	FC-404-2005

Quant-iT™ Pico Green®	Thermo Fisher Scientific Inc.	Cat# P7589
ABsolute QPCR SYBR Green Mix (no ROX)	Thermo Fisher Scientific	Cat# AB-1158/B
PowerUp™ SYBR® Green Master Mix	Thermo Fisher Scientific	Cat# A25778
Deposited Data		
Raw and analyzed data	This paper	GEO: GSE78957
Raw data N-MYC depleted neuroblastoma cells	Valentijn LJ et al., 2012	GEO: GSE39218
Expression data at different stages of neuroblastoma	R. Versteeg	GEO: GSE16476
Experimental Models: Cell Lines		
Human neuroblastoma: IMR-5	A. Eggert	N/A
Human neuroblastoma: IMR-32	M. Schwab	N/A
Human neuroblastoma: SH-EP	M. Schwab	N/A
Human neuroblastoma: SH-EP NMYCER	M. Eilers	N/A
Pseudoviral Particle Producer cell line: HEK293TN	ATCC	Cat# CRL-11268
Retroviral Packaging cell line: PlatE	B. v. Eyss	N/A
Recombinant DNA		
pInducer-11	Addgene	Cat# 44363 Meerbrey et al., 2011
psPAX.2	Addgene	Cat# 12260 D. Trono
pMD2.G	Addgene	Cat# 12259 D. Trono
pETM6T1	R. Bayliss	N/A
lentiCRISPR v2	Addgene	Cat# 52961 Sanjana et al., 2014
Sequence-Based Reagents		
ON-TARGETplus SMARTpools GTF3C5	GE Healthcare	L-020031-00-0005
ON-TARGETplus SMARTpools RAD21	GE Healthcare	L-006832-00-0005
ON-TARGETplus non-targeting control pool	GE Healthcare	D-001810-10-20
shRNA targeting TFIIIC5: AAGCGCAGCACCTACAACTACA	(Fellmann et al., 2013)	shRNA ID: GTF3C5.1361
shRNA targeting TFIIIC2: TCCGTAGAGATGTCATTACCTA	Fellmann et al., 2013	shRNA ID: GTF3C2.435

shRNA targeting N-MYC: GAGGAGCATGTTTTGTATACAA	Fellmann et al., 2013	shRNA ID: MYCN.2214
Primers for ChIP, see Supplemental Experimental Procedures	This paper	N/A
gRNA for CRISPR, see Supplemental Experimental Procedures	Hart et al., 2015	N/A
Software and Algorithms		
Bowtie v1.1.1	Langmead and Salzberg, 2012	
MACS v1.4.2	Zhang et al., 2008	
Integrated Genome Browser	Nicol et al., 2009	
SeqMINER	Ye et al., 2014	
BEDTools	Quinlan, 2014	
MEME Suite	Bailey et al., 2009	
TopHat2	Kim et al., 2003	
GSEA	Subramanian et al., 2005	
DeepTools	Ramirez et al., 2016	
Ngs.plot	Shen et al., 2014	
Prism5.0 Software	GraphPad	

References

BAILEY, T. L., BODEN, M., BUSKE, F. A., FRITH, M., GRANT, C. E., CLEMENTI, L., REN, J., LI, W. W. & NOBLE, W. S. 2009. MEME SUITE: tools for motif discovery and searching. *Nucleic Acids Res,* 37**,** W202-8.

BAYLISS, R., SARDON, T., VERNOS, I. & CONTI, E. 2003. Structural basis of Aurora-A activation by TPX2 at the mitotic spindle. *Mol Cell,* 12**,** 851-62.

BURGESS, S. G. & BAYLISS, R. 2015. The structure of C290A:C393A Aurora A provides structural insights into kinase regulation. *Acta Crystallogr F Struct Biol Commun,* 71**,** 315-9.

CHEN, X., XU, H., YUAN, P., FANG, F., HUSS, M., VEGA, V. B., WONG, E., ORLOV, Y. L., ZHANG, W., JIANG, J., LOH, Y. H., YEO, H. C., YEO, Z. X., NARANG, V., GOVINDARAJAN, K. R., LEONG, B., SHAHAB, A., RUAN, Y., BOURQUE, G., SUNG, W. K., CLARKE, N. D., WEI, C. L. & NG, H. H. 2008. Integration of external signaling pathways with the core transcriptional network in embryonic stem cells. *Cell,* 133**,** 1106-17.

COX, J. & MANN, M. 2008. MaxQuant enables high peptide identification rates, individualized p.p.b.-range mass accuracies and proteome-wide protein quantification. *Nat Biotechnol,* 26**,** 1367-72.

FELLMANN, C., HOFFMANN, T., SRIDHAR, V., HOPFGARTNER, B., MUHAR, M., ROTH, M., LAI, D. Y., BARBOSA, I. A., KWON, J. S., GUAN, Y., SINHA, N. & ZUBER, J. 2013. An optimized microRNA backbone for effective single-copy RNAi. *Cell Rep,* 5**,** 1704-13.

HART, T., CHANDRASHEKHAR, M., AREGGER, M., STEINHART, Z., BROWN, K. R., MACLEOD, G., MIS, M., ZIMMERMANN, M., FRADET-TURCOTTE, A., SUN, S., MERO, P., DIRKS, P., SIDHU, S., ROTH, F. P., RISSLAND, O. S., DUROCHER, D., ANGERS, S. & MOFFAT, J. 2015. High-Resolution CRISPR Screens Reveal Fitness Genes and Genotype-Specific Cancer Liabilities. *Cell,* 163**,** 1515-26.

JAENICKE, L. A., VON EYSS, B., CARSTENSEN, A., WOLF, E., XU, W., GREIFENBERG, A. K., GEYER, M., EILERS, M. & POPOV, N. 2016. Ubiquitin-Dependent Turnover of MYC Antagonizes MYC/PAF1C Complex Accumulation to Drive Transcriptional Elongation. *Mol Cell,* 61**,** 54-67.

KIM, D., PERTEA, G., TRAPNELL, C., PIMENTEL, H., KELLEY, R. & SALZBERG, S. L. 2013. TopHat2: accurate alignment of transcriptomes in the presence of insertions, deletions and gene fusions. *Genome Biol,* 14**,** R36.

LANGMEAD, B. & SALZBERG, S. L. 2012. Fast gapped-read alignment with Bowtie 2. *Nat Methods,* 9**,** 357-9.

NICOL, J. W., HELT, G. A., BLANCHARD, S. G., JR., RAJA, A. & LORAINE, A. E. 2009. The Integrated Genome Browser: free software for distribution and exploration of genome-scale datasets. *Bioinformatics,* 25**,** 2730-1.

NORTH, B. V., CURTIS, D. & SHAM, P. C. 2002. A note on the calculation of empirical P values from Monte Carlo procedures. *Am J Hum Genet,* 71**,** 439-41.

QUINLAN, A. R. 2014. BEDTools: The Swiss-Army Tool for Genome Feature Analysis. *Curr Protoc Bioinformatics,* 47**,** 11 12 1-11 12 34.

RAHL, P. B., LIN, C. Y., SEILA, A. C., FLYNN, R. A., MCCUINE, S., BURGE, C. B., SHARP, P. A. & YOUNG, R. A. 2010. c-Myc regulates transcriptional pause release. *Cell,* 141**,** 432-45.

RAMIREZ, F., RYAN, D. P., GRUNING, B., BHARDWAJ, V., KILPERT, F., RICHTER, A. S., HEYNE, S., DUNDAR, F. & MANKE, T. 2016. deepTools2: a next generation web server for deep-sequencing data analysis. *Nucleic Acids Res,* 44**,** W160-5.

SCHULEIN-VOLK, C., WOLF, E., ZHU, J., XU, W., TARANETS, L., HELLMANN, A., JANICKE, L. A., DIEFENBACHER, M. E., BEHRENS, A., EILERS, M. & POPOV, N. 2014. Dual regulation of fbw7 function and oncogenic transformation by usp28. *Cell Rep,* 9**,** 1099-109.

SHEN, L., SHAO, N., LIU, X. & NESTLER, E. 2014. ngs.plot: Quick mining and visualization of next-generation sequencing data by integrating genomic databases. *BMC Genomics,* 15**,** 284.

SUBRAMANIAN, A., TAMAYO, P., MOOTHA, V. K., MUKHERJEE, S., EBERT, B. L., GILLETTE, M. A., PAULOVICH, A., POMEROY, S. L., GOLUB, T. R., LANDER, E. S. & MESIROV, J. P. 2005. Gene set enrichment analysis: a knowledge-based approach for interpreting genome-wide expression profiles. *Proc Natl Acad Sci U S A,* 102**,** 15545-50.

VON EYSS, B., JAENICKE, L. A., KORTLEVER, R. M., ROYLA, N., WIESE, K. E., LETSCHERT, S., MCDUFFUS, L. A., SAUER, M., ROSENWALD, A., EVAN, G. I., KEMPA, S. & EILERS, M. 2015. A MYC-Driven Change in Mitochondrial Dynamics Limits YAP/TAZ Function in Mammary Epithelial Cells and Breast Cancer. *Cancer Cell,* 28**,** 743-57.

WALZ, S., LORENZIN, F., MORTON, J., WIESE, K. E., VON EYSS, B., HEROLD, S., RYCAK, L., DUMAY-ODELOT, H., KARIM, S., BARTKUHN, M., ROELS, F., WUSTEFELD, T., FISCHER, M., TEICHMANN, M., ZENDER, L., WEI, C. L., SANSOM, O., WOLF, E. & EILERS, M. 2014. Activation and repression by oncogenic MYC shape tumour-specific gene expression profiles. *Nature,* 511**,** 483-7.

YE, T., RAVENS, S., KREBS, A. R. & TORA, L. 2014. Interpreting and visualizing ChIP-seq data with the seqMINER software. *Methods Mol Biol,* 1150**,** 141-52.

ZHANG, Y., LIU, T., MEYER, C. A., EECKHOUTE, J., JOHNSON, D. S., BERNSTEIN, B. E., NUSBAUM, C., MYERS, R. M., BROWN, M., LI, W. & LIU, X. S. 2008. Model-based analysis of ChIP-Seq (MACS). *Genome Biol,* 9**,** R137.

Figure S1 Büchel et al.

A

Gene name	log_2 Ratio wt vs. Ctr	log_2 Ratio mut vs. Ctr	Reference
MYCN	10.88	10.31	NA
EP400	8.99	8.47	Fuchs, M. et al., Cell (2001).
TRRAP	7.75	8.43	McMahon, S.B. et al., Cell (1998).
MAX	7.61	5.65	Blackwood, E.M. & Eisenman, R.N., Science (1991).
DMAP1	5.08	5.68	Cai, Y. et al., JBiolChem (2005).
BPTF	4.90	3.91	Richart, L. et al., Nat Commun (2016).
CDC73	4.14	4.29	Jaenicke, L.A. et al., Mol Cell (2016).
VPS72	3.70	3.81	Cai, Y. et al., JBiolChem (2005).
MYCBP2	3.33		Guo, Q. et al., PNAS (1998).
HCFC1	3.56	3.03	Thomas, L.R. et al., Oncogene (2016).
YEATS4	3.33	2.84	Piccinni, E. et al., Acta Biochim Pol (2011).
EPC1	3.08	2.37	Doyon, Y et al., Molecular and cellular biology (2004).
PAF1	2.77	2.66	Jaenicke, L.A. et al., Mol Cell (2016).
PLK1	2.34	2.96	Popov, N. et al., Nature cell biology (2010).
CCNT1	2.48		Eberhardy, S.R. & Farnham, P.J., JBiolChem (2002).
KAT5	2.41	2.40	Frank, S.R. et al., EMBO Rep (2003).
AURKA	2.25		Otto, T. et al., Cancer Cell (2009).
RUVBL2	1.46	1.50	Wood, M.A. et al., Mol Cell (2000).
RUVBL1	1.30	1.53	Wood, M.A. et al., Mol Cell (2000).

C

	Unique peptide counts	
Gene name	N-MYC IP	Ctr
MYCN	83	0
TRRAP	54	0
GTFIIIC1	39	0
HCFC1	15	0
GTFIIIC3	13	0
GTFIIIC4	8	0
GTFIIIC5	8	0
GTFIIIC2	7	2
TOP2A	4	0

D

	Unique peptide counts	
Gene name	MYC IP	Ctr
MYC	30	1
TRRAP	109	2
GTFIIIC1	16	5
GTFIIIC3	10	2
GTFIIIC5	8	2
GTFIIIC2	5	3
TOP2A	23	10

B

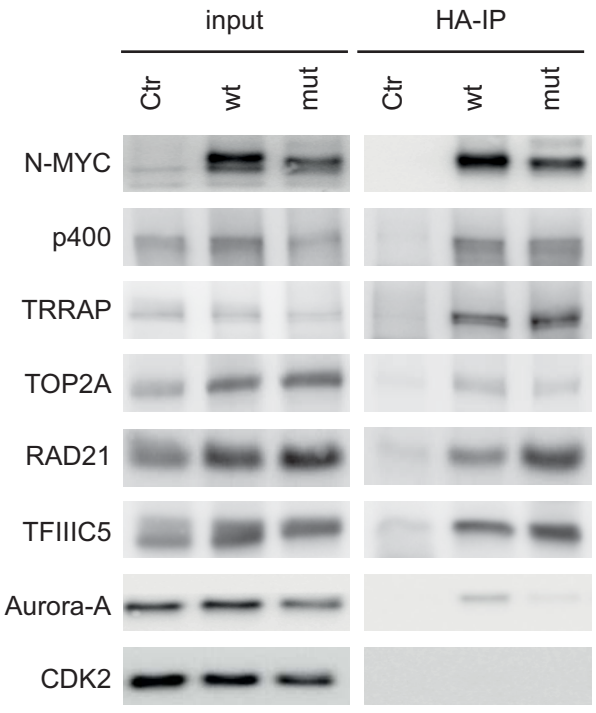

E

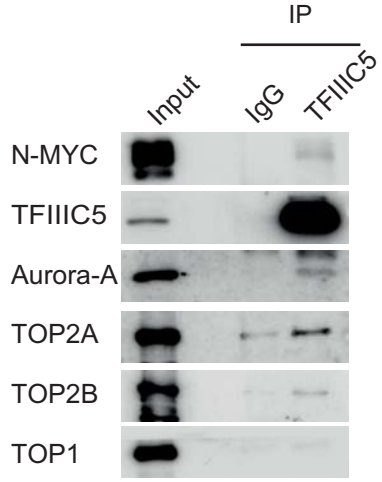

F

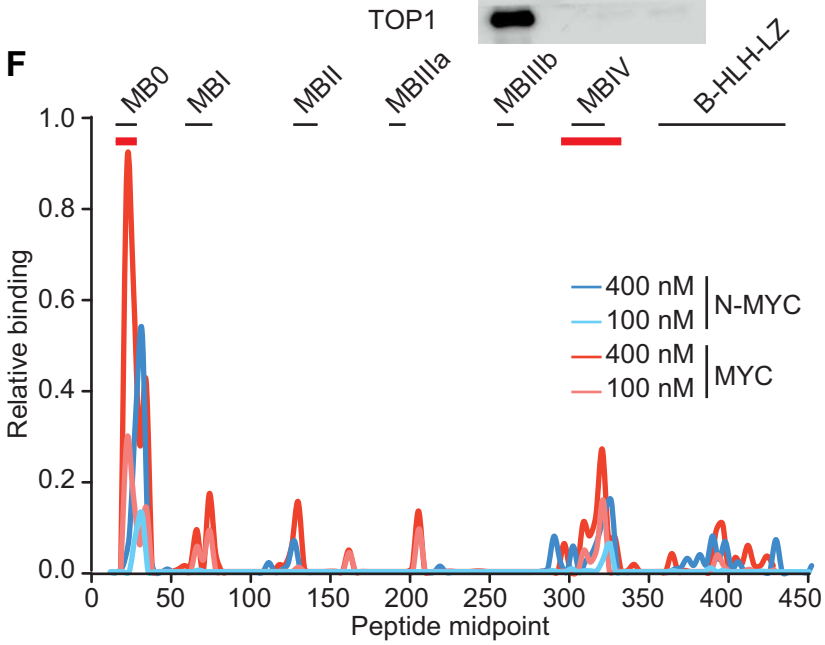

Figure S1: Related to Figure 1.

A. Table of previously identified protein-protein interactions of MYC and N-MYC proteins that were confirmed by our analysis. The table shows normalized $\log_2$ ratios of peptides purified from SH-EP cells expressing HA-tagged N-MYC_{wt} (wt) or N-MYC_{mut} (mut) relative to empty control vector (Ctr).

B. Immunoblots of α-HA immunoprecipitates from SH-EP cells expressing HA-tagged N-MYC_{wt} or N-MYC_{mut} or an empty control vector (Ctr). The input corresponds to 1% of the amount used for precipitation.

C. Table of mass spectrometry results of N-MYC immunoprecipitates from *MYCN*-amplified Kelly cells. Shown are peptide numbers of the indicated proteins.

D. Table of mass spectrometry results of MYC immunoprecipitates from U2OS cells expressing HA-tagged MYC. Shown are peptide numbers of the indicated proteins.

E. Immunoblots of α-TF3C5 immunoprecipitates from IMR-5 cells. The input corresponds to 1% of the amount used for precipitation. Non-specific IgG was used for control immunoprecipitation.

F. Peptide arrays showing binding of Aurora-A to peptide microarrays of N-MYC and MYC. 23mer peptides were spotted, each shifted by 5 amino acids. X-axis shows the position of peptide midpoints and the y-axis shows relative binding. Positions of conserved domains ("MYCboxes") are indicated at the top of the graph. Data are shown for two concentrations of Aurora-A.

Figure S2 Büchel et al.

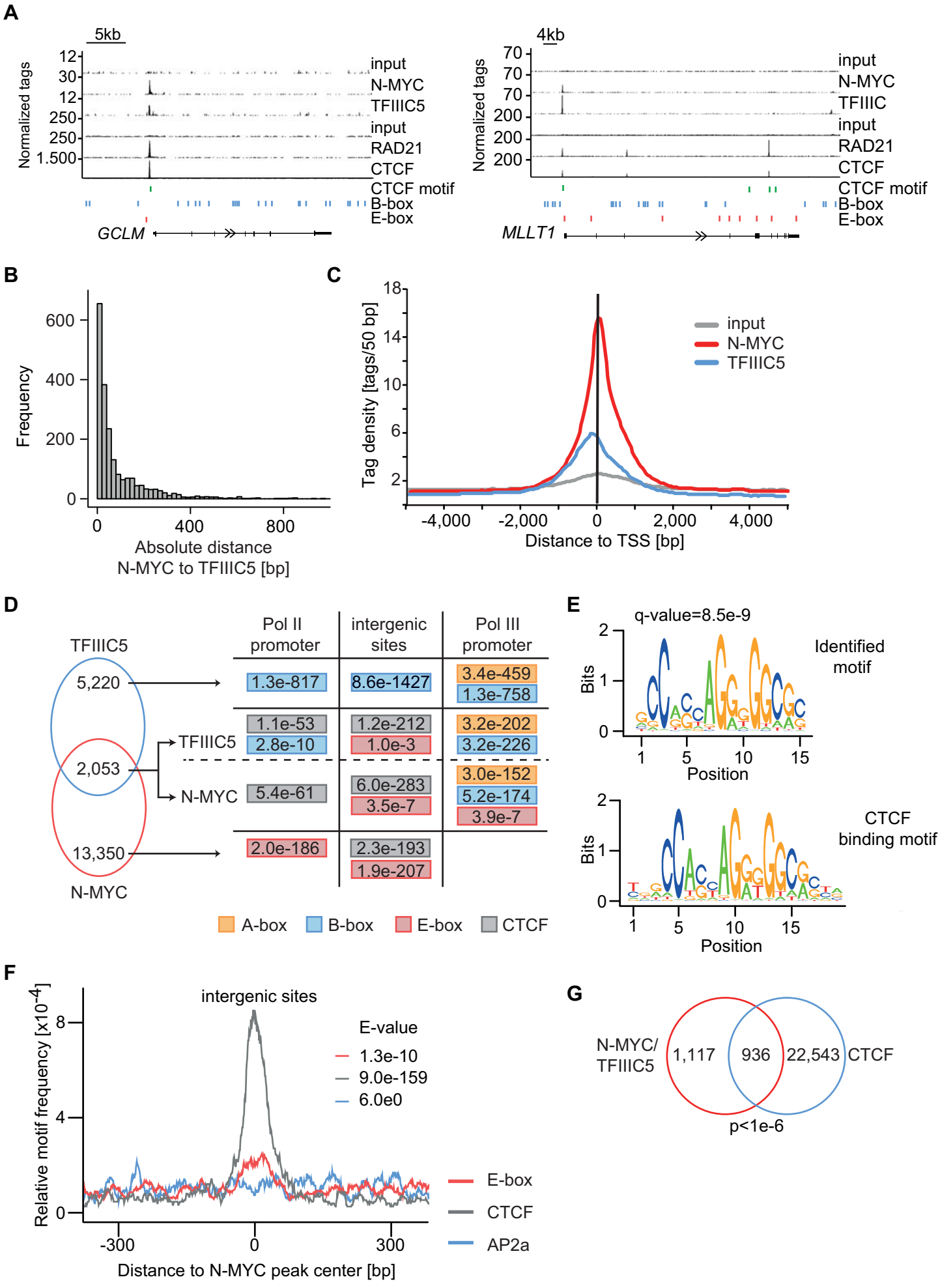

Figure S2: Related to Figure 2.

A. Genome browser tracks at the *GCLM* and *MLLT1* loci illustrating DNA-binding of the indicated proteins. ChIP sequencing was performed on *MYCN*-amplified IMR-5 cells. The positions of B- and E-boxes and of CTCF motifs are indicated by vertical lines. Upper input is for ChIP sequencing of N-MYC and TFIIIC5, lower input for ChIP sequencing of RAD21 and CTCF.

B. Histogram demonstrating absolute distance between N-MYC and TFIIIC5 peak summits of N-MYC/TFIIIC5 joint peaks (n=2,053). The histogram is plotted at a resolution of 20 bp.

C. Tag density distribution of N-MYC and TFIIIC5 at overlapping sites around the transcription start site (TSS) of genes transcribed by Pol II.

D. *De novo* motif search in N-MYC- and/or TFIIIC5-bound regions. E-values were calculated using a binominal test and normalized to the number motifs in the database and are shown only if the respective motif was enriched in the bound sequences.

E. Sequence and q-value of the *de novo* identified motif in overlapping N-MYC/TFIIIC sites and comparison to a published CTCF motif (JASPAR MA0139.1).

F. Central enrichment of E-box, CTCF and AP2a (as negative control) motifs in the N-MYC peak of N-MYC/TFIIIC5 joint sites in intergenic sites. The E-value is calculated by a binominal test and adjustment for the number of motifs tested.

G. Venn diagram documenting genome-wide overlap of N-MYC/TFIIIC5 joint binding sites with CTCF. The p-value was calculated using a permutation test with 100,000 iterations.

Figure S3 Büchel et al.

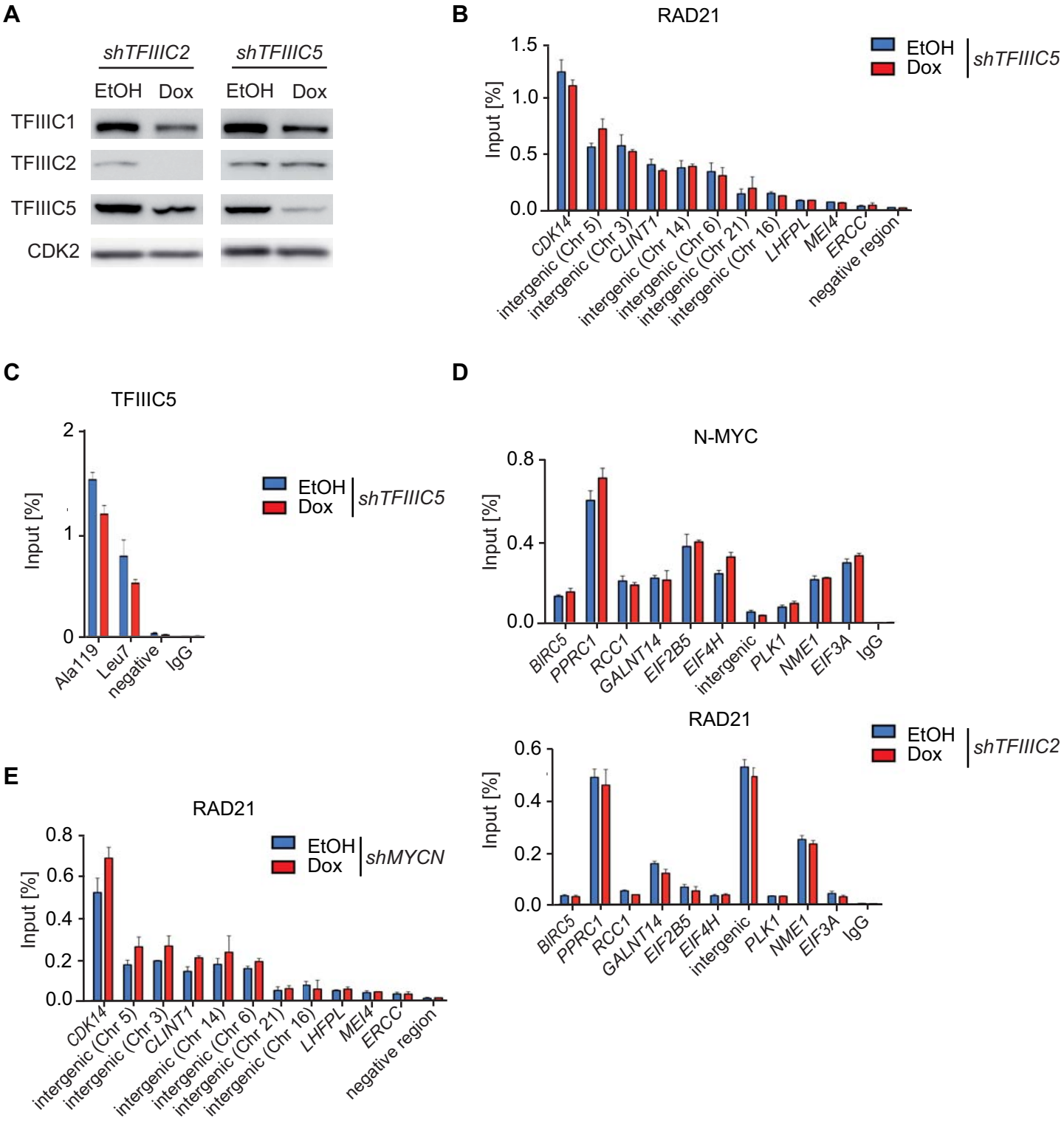

Figure S3: Related to Figure 3.

A. Immunoblot showing levels of the indicated proteins in response to depletion of TFIIIC2 or TFIIIC5. IMR-5 cells expressing an inducible shRNA directed against TFIIIC2 or TFIIIC5 were treated with doxycycline (Dox) for 48 hr or with ethanol (EtOH) as control.

B. ChIP experiment documenting binding of RAD21 to the indicated loci upon depletion of TFIIIC5. Error bars show SD of technical triplicates. These binding sites contain no detectable TFIIIC5 or N-MYC peak.

C. ChIP experiment showing binding of TFIIIC5 to tRNA genes upon depletion of TFIIIC5. Error bars show SD of technical triplicates from one experiment (n = 2).

D. ChIP experiment documenting binding of N-MYC and RAD21 to the indicated loci upon depletion of TFIIIC2. Error bars show SD of technical triplicates from one representative experiment (n = 3).

E. ChIP experiment documenting binding of RAD21 to the indicated loci upon depletion of N-MYC. Error bars show SD of technical triplicates. These binding sites contain no detectable TFIIIC5 or N-MYC peak

Figure S4 Büchel et al.

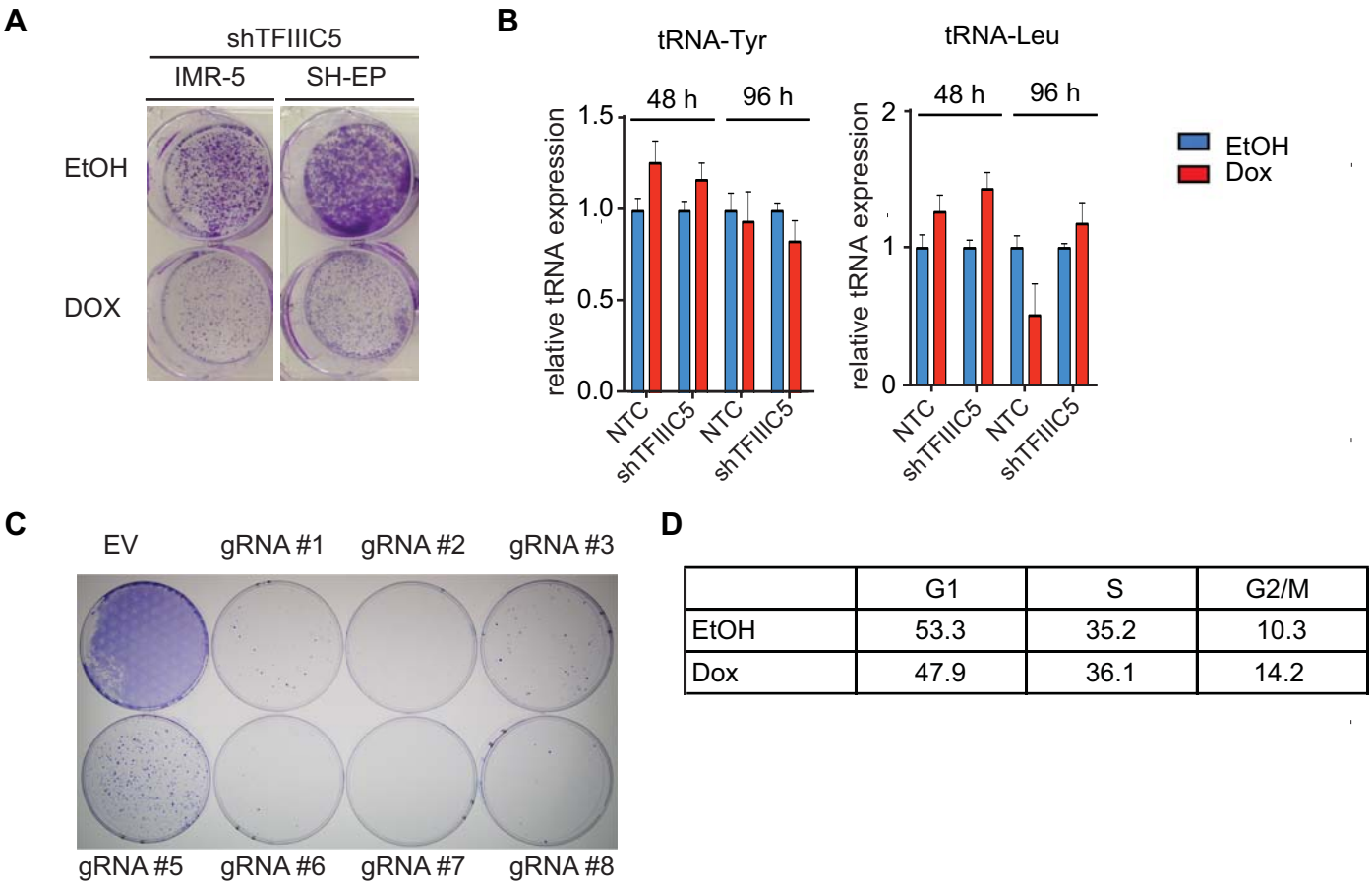

	G1	S	G2/M
EtOH	53.3	35.2	10.3
Dox	47.9	36.1	14.2

Figure S4: Related to Figure 4.

A. Clonogenic assay of IMR-5 and SH-EP neuroblastoma cells after shRNA-mediated knockdown of TFIIIC5. Colonies were stained with crystal violet.

B. Expression of indicated tRNAs in IMR-5 cells after shRNA-mediated depletion of TFIIIC5 or a non targeting control (NTC). Doxycycline or ethanol was added for 48 hr or 96 hr as indicated. Error bars show SD of technical triplicates.

C. Clonogenic assay of IMR-5 cells after sgRNA-mediated knockout of TFIIIC5. Colonies were stained with crystal violet. Multiple independent gRNA sequences were used.

D. Cell cycle distribution of IMR-5 cells after shRNA-mediated depletion of TFIIIC5. Data are taken from a propidium-iodide stained FACS experiment of cells before and 48 hr after addition of doxycycline.

Figure S5 Büchel et al.

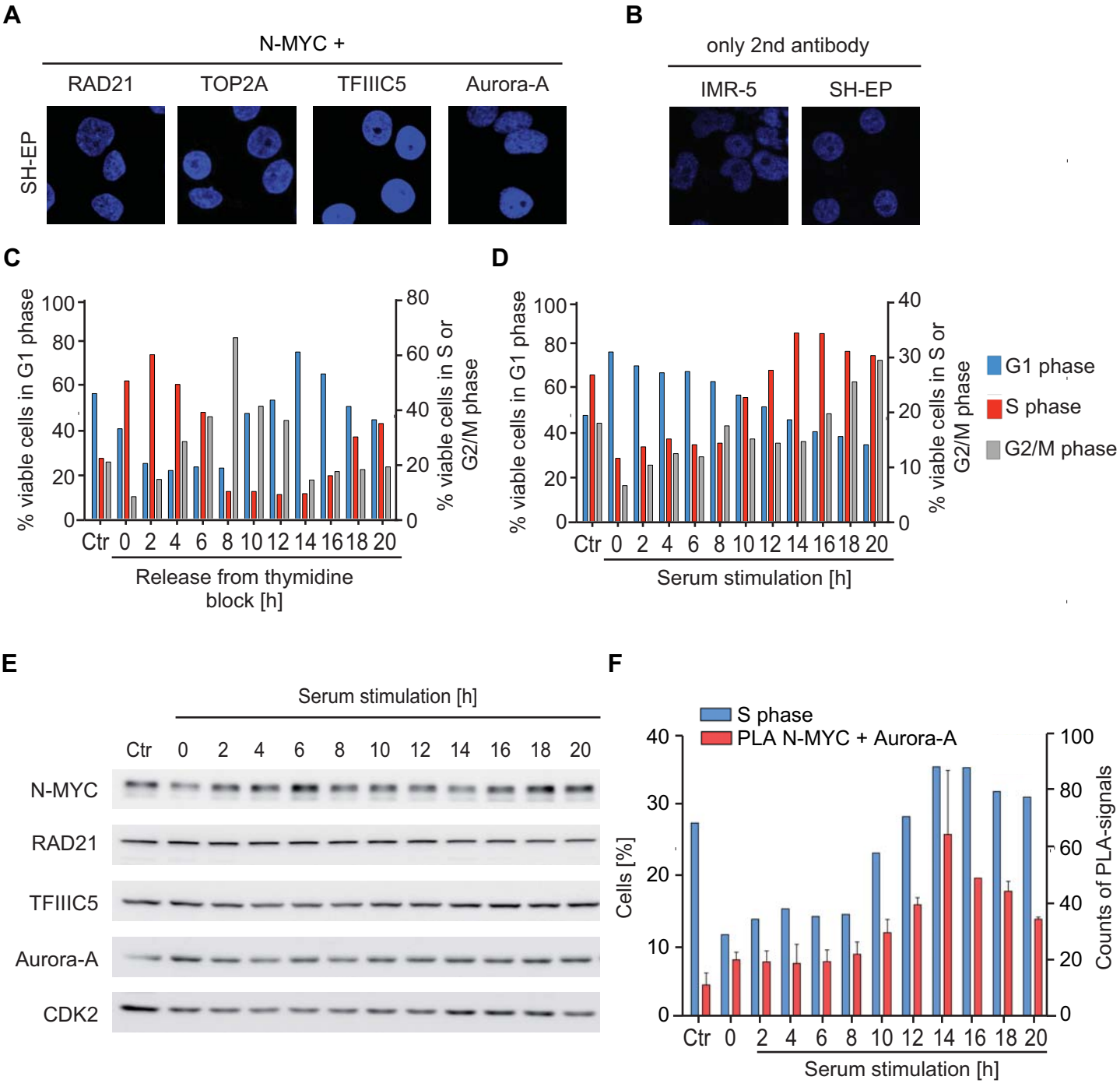

Figure S5: Related to Figure 5.

A. Negative controls for PLAs from SH-EP cells. The indicated antibodies were added to SH-EP cells that do not express N-MYC. Nuclei are stained using Hoechst.

B. Negative controls for PLAs from IMR-5 and SH-EP cells. The panels show PLA assays in which cells were incubated with secondary antibody only. Nuclei are stained using Hoechst.

C. Cell cycle distribution as determined by PI-FACS after release of IMR-5 cells from a double-thymidine block for the indicated times (n = 5). Left axis refers to viable cells in G1 phase shown in blue. Right axis refers to viable cells in S phase shown in red as well as G2/M phase shown in grey.

D. Cell cycle distribution as determined by PI-FACS after re-stimulation of serum-starved IMR-5 cells with 10% FCS (n = 5). Coloring is as in panel C.

E. Immunoblots documenting the levels of the indicated proteins re-stimulation of serum-starved IMR-5 cells with 10% FCS (n = 4).

F. Quantification of the PLA assay between N-MYC and Aurora-A after re-stimulation of serum-starved cells. The percentage of cells in S phase from one representative experiment is indicated in parallel. Error bars show SD of technical triplicates (n = 3).

G. The panels show representative pictures from PLAs documenting complex formation between N-MYC and the indicated proteins (n = 2). Nuclei are stained using Hoechst. Red dots show PLA signals resulting from interactions of N-MYC and the indicated proteins.

H. PLA assays documenting complex formation between N-MYC and TFIIIC5 after release from a double-thymidine block (n = 3). Nuclei are stained using Hoechst. Red dots show PLA signal for interaction of N-MYC and TFIIIC5.

Figure S6 Büchel et al.

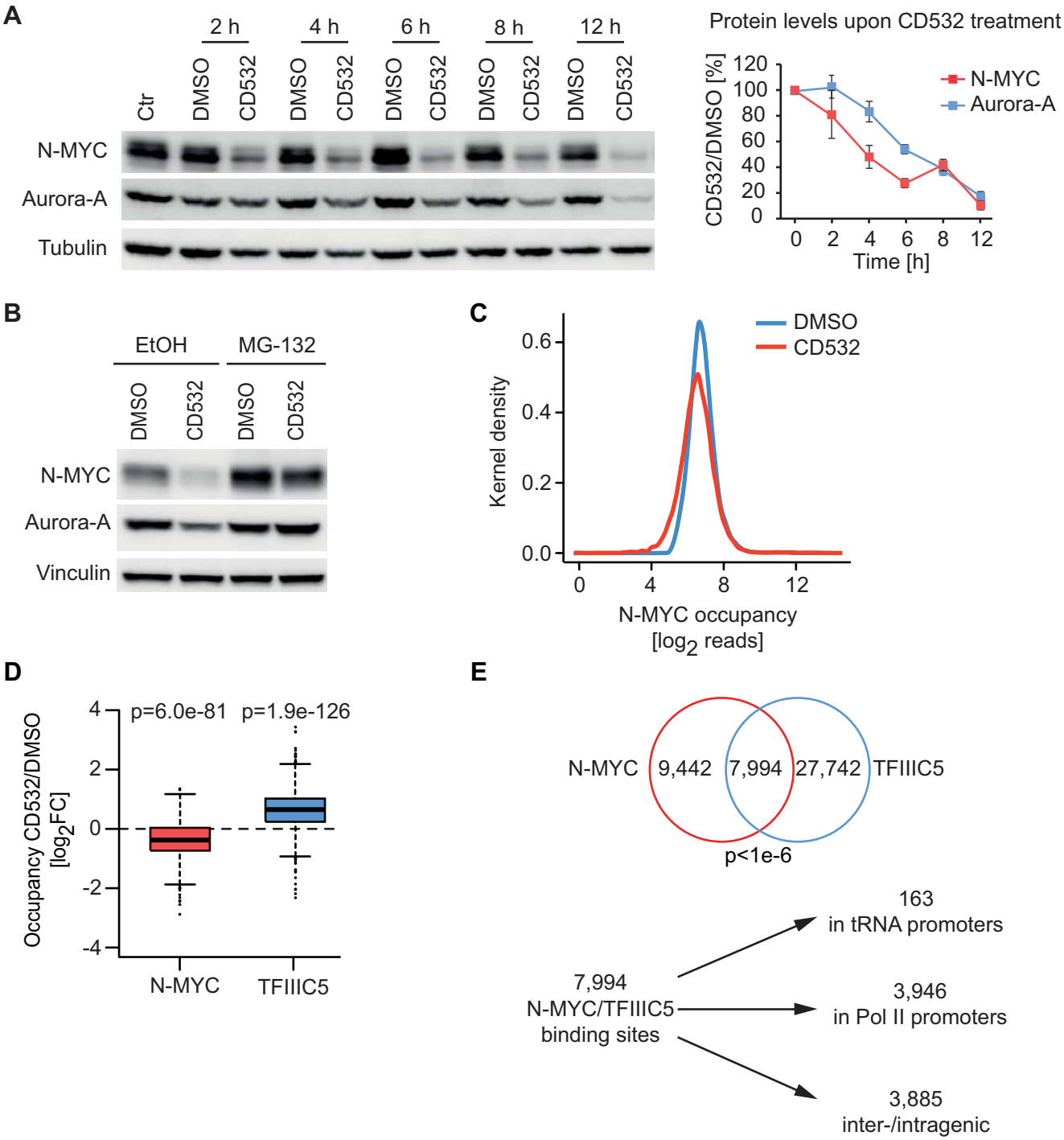

Figure S6: Related to Figure 6.

A. Immunoblots (left) and quantification (right) documenting decrease in overall N-MYC and Aurora-A levels after exposure of IMR-5 cells to CD532 (1 μM) for the indicated times. Error bars show SD (n = 3).

B. Immunoblot documenting levels of Aurora-A and N-MYC after 4 hr exposure to 1 μM of CD532 in the presence of the proteasome inhibitor MG-132 or ethanol (EtOH) as control (n = 2).

C. Change in N-MYC occupancy upon CD532 treatment of all N-MYC peaks (n=15,403). Reads were counted in a window of 250 bp around the peak summit, $\log_2$-transformed and the probability density estimation was calculated using a Gaussian kernel function with a bandwidth of 0.1.

D. Box plots documenting changes in N-MYC and TFIIIC5 occupancy at overlapping binding sites in Pol II promoters after exposure of non-synchronized IMR-5 cells to CD532 (4 hr; 1 μM).

E. Venn diagram documenting genome-wide overlap of N-MYC and TFIIIC5 in IMR-5 neuroblastoma cells after exposure to CD532. The p-value was calculated using a permutation test with 100,000 iterations (top). Diagram showing distribution of joint N-MYC/TFIIIC5 binding sites (bottom).

F. Mean tag density around 28,671 TFIIIC5 binding sites without an overlapping N-MYC peak. Tags were counted in a window of +/-1.5 kb around the TFIIIC5 peak summit at a resolution of 50 bp.

Figure S7 Büchel et al.

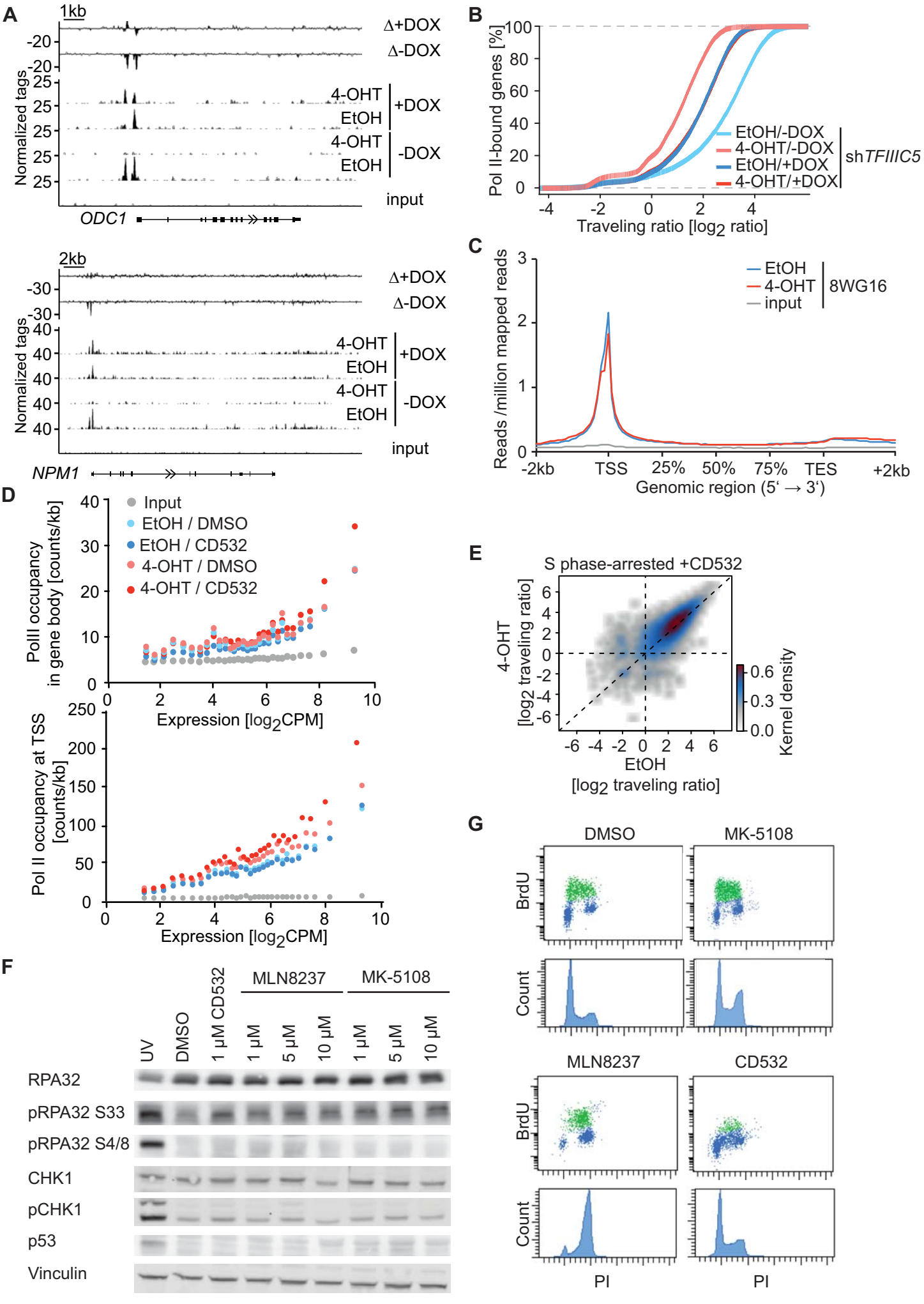

Figure S7: Related to Figure 7.

A. Browser plots showing Pol II occupancy at the indicated loci in SHEP-N-MYCER cells expressing a doxycycline-inducible shRNA targeting TFIIIC5. Doxycycline (1 µg ml^{-1}) was added for 30 hr where indicated, EtOH was used as control. The top two traces show N-MYC induced changes (∆) in Pol II occupancy in control and in TFIIIC5-depleted cells.

B. Empirical distribution function (ECDF) plot showing changes in Pol II traveling ratio under the indicated conditions.

C. Metagene plot of all expressed genes (n=14,650) illustrating distribution of hypo-phosphorylated Pol II (8WG16) within transcribed regions before and five hours after activation of N-MYCER.

D. Occupancy of Pol II in the gene body (top) and at the TSS (bottom) sorted according to gene expression in IMR-5 cells synchronized in S phase and treated with CD532 where indicated. Only expressed genes were used (n=14,927) and 30 equal-sized bins (each representing 500 genes) were calculated using the arithmetic mean.

E. 2D Kernel density blot showing Pol II traveling ratio in S phase arrested cells after two hours of CD532 treatment before and after four hours of N-MYCER-activation.

F. Effect of Aurora-A inhibitors on phosphorylation of the indicated proteins in IMR-5 cells synchronized in S phase. Inhibitors were added for 2 hours in indicated concentrations (n = 4).

G. FACS analysis documenting altered DNA synthesis upon incubation of IMR-5 cells with MK- 5108, CD532 and MLN8237. Upper panels show BrdU/propidium iodide double staining (with BrdU-positive cells marked in green), lower panels show propidium iodide.